New Techniques For The Measurement of X-Ray Beam or X-Ray Optics Quality

Ph. Zeitoun [1], Ph. Balcou [2], S. Bucourt [3], D. Benredjem [1], F. Delmotte [4], G. Dovillaire [3], D. Douillet [2], J. Dunn [5], G. Faivre [1], M. Fajardo [1], K.A. Goldberg [6], M. Idir [1], S. Hubert [2,1], J. R. Hunter [5], S. Jacquemot [7], S. Kazamias [2], S. le Pape [1], X. Levecq [3], C.L.S. Lewis [8], R. Marmoret [7], P. Mercère [1], A.S. Morlens [1], P.P. Naulleau [6], C. Rémond [7], J. J. Rocca [9], S. Sebban [2], R. F. Smith [5], M. F. Ravet [4], P. Troussel [7], C. Valentin [2] and L. Vanbostal [1].

[1] Laboratoire d'Interaction du rayonnement X avec la Matière, Université Paris-Sud, Bât 350, 91405 Orsay, France.
[2] Laboratoire d'Optique Appliquée, ENSTA-Ecole Polytechnique, Chemin de La Hunière, 91761 Palaiseau, France
[3] Imagine Optic, 18 rue Charles de Gaulle, 91400 Orsay , France
[4] Laboratoire Charles Fabry de l'Institut d'Optique, Université Paris-Sud, France
[5] Lawrence Livermore National Laboratory, Livermore, CA 94551
[6] Center for X-Ray Optics, Ernest Orlando Lawrence Berkeley National Laboratory, 1 Cyclotron Road, Berkeley, CA 94720
[7] Commisariat á l'Énergie Atomique, BP 2, 91680 Bruyères-le-Chatel, France.
[8] School of Mathematics and Physics, The Queen's University of Belfast, Belfast BT7 1NN, UK.
[9] Department of Electrical and Computer Engineering, Colorado State University, Fort Collins, CO 80523-1373

ABSTRACT

Metrology of XUV beams and more specifically X-ray laser (XRL) beam is of crucial importance for development of applications. We have then developed several new optical systems enabling to measure the x-ray laser optical properties. By use of a Michelson interferometer working as a Fourier-Transform spectrometer, the line shapes of different x-ray lasers have been measured with an unprecedented accuracy ($\delta\lambda/\lambda\sim10^{-6}$). Achievement of the first XUV wavefront sensor has enable to measure the beam quality of laser-pumped as well as discharge pumped x-ray lasers. Capillary discharge XRL has demonstrated a very good wavefront allowing to achieve intensity as high $3*10^{14}$ Wcm^{-2} by focusing with a f = 5 cm mirror. The measured sensor accuracy is as good as $\lambda/120$ at 13 nm. Commercial developments are under way.

Keywords: x-ray laser, longitudinal coherence, Michelson soft x-ray interferometry, EUV optics

1. INTRODUCTION

Since the early development of laboratory x-ray lasers, the achievement of applications has been considered as the main objective. Most recently, the emergence of several X-ray laser facilities (COMET, JAERY, LASERIX) strongly reinforced the actual trend to use x-ray lasers (XRL) for applications but with a versatility comparable to visible laser one. However due to the wavelength shortening, the development of applications requires to have better and better XUV optics (wavelength range 10-60 nm typically), from individual mirrors to more sophisticated set-ups like interferometers. A novel trend appears very recently with XRL facilities : on-line metrology of x-ray laser beam. Due to the diversity of applications, the metrology must cover a wide range of beam parameters from shot-to-shot energy up to

wavefront measurement. This paper will describe the most recent works achieved on XRL beam metrology at the Laboratoire d'Interaction du rayonnement X avec la Matière (LIXAM) through several collaborations.

2. XUV FOURIER-TRANSFORM SPECTROSCOPY USING A MICHELSON INTERFEROMETER.

From the first experiments of L. B. da Silva [1] and collaborators or D. Joyeux and co-workers [2], many interferometers have been setting-up (Mach-Zehnder, Fresnel bimirror, Lloyds [3], SMARTT [4]…). At LIXAM, we have chosen to develop the so-called Michelson interferometer. This interferometer has been chosen for two main reasons. First the geometry allows to easily and under vacuum change the fringes parameters, i.e. spacing and orientations. This is an important improvement compared to previous interferometers. As a matter of example, while probing a plasma the strong variation of the density gradients may locally cause a fringe mixing preventing from retrieving the phase and then the density. The solution consists to increase the fringe spacing which is most often done by fully re-aligning the interferometer. This may take several hours or days, while with the Michelson it is done under vacuum by simply tilting a mirror with a motorized stage. The second reason for preferring the Michelson interferometer is coming from its common use, in visible wavelength range, as a highly resolving spectrometer. We will concentrate this part of the paper on that technique called Fourier-Transform spectroscopy, based on the Michelson interferometer. More precisely, we have used the Michelson interferometer for measuring the line shape (and not only the line-width) of several X-ray lasers, typically pumped by 130 ps or 10 ps lasers.

The method of deducing spectral lines by recording the intensity of interference fringes was pioneered by A. A. Michelson in 1891 [5]. By smoothly translating one end-mirror of this interferometer (fig.1) the optical path difference δ between the beams reflecting off the two mirrors varied continuously producing an interferogram. The fringe visibility, V, that we measure is equal to the magnitude of the complex degree of temporal coherence, $\gamma(\tau)$, of the illumination beam. This latter quantity is directly related to the power spectral density $J(\nu)$ of the beam through a Fourier-transform relation (Wiener-Khinchin theorem [6]) :

$$J(\nu) = \int_0^\infty \gamma(\tau) \cdot e^{i2\pi\nu\tau} d\tau$$

where τ (= δ/c) is the relative time delay. Consequently, obtaining the Fourier-transform of the variation of fringe visibility versus optical path difference allows us to deduce the spectral line shape of a given source. Straightforward we may remark that the easiness of changing the Michelson interferometer set-up is crucial here for scanning the contrast curve.
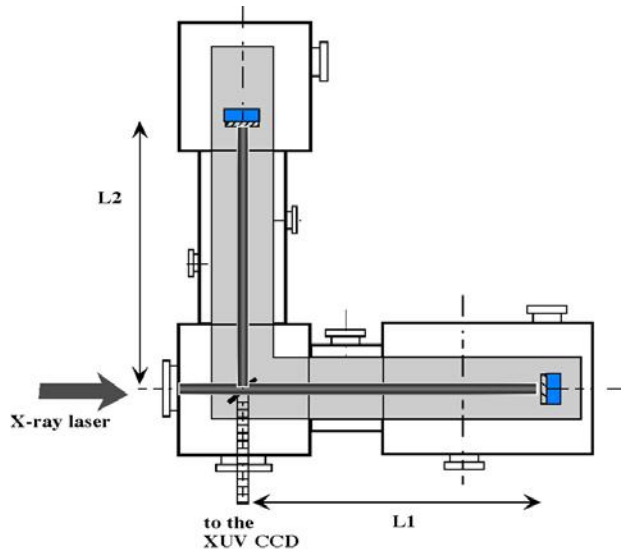

Figure 1 : Schematic drawing of the Michelson interferometer set up for the LULI experiment. L1 and L2 are the path lengths for each arm.

This first study was performed with the 13.89 nm, collisionally excited, Ni-like silver XRL running at the Laboratoire pour l'Utilisation des Lasers Intenses (LULI) in France. The XRL was produced by irradiating a massive, 2 cm wide, silver target with six IR beams ($\lambda = 1.054$ µm, $\Delta t_{FWHM} = 130$ ps) at an intensity on target of 3×10^{13} Wcm^{-2}. The highly ionized laser-produced plasma undergoes a population inversion by electronic collisional excitation. Spontaneously emitted rays are then amplified in single pass by travelling along the whole plasma column. The XRL has an output energy ranging from 50 to 400 µJ [7], a measured divergence near 1.9×5 mrad^2 and a refraction angle of 4 mrad in the horizontal plane. Displayed below are two interferograms obtained for equilibrated arms (2a) and with a path length difference of 200 µm (2b). We may observe that the fringes are straight over the major part of the view field but being distorted on the edges. As one can see on figure 1, the Michelson interferometer is composed of two flat mirrors, with relatively good flatness, and a beamsplitter. This element is the most critical since it is composed of a thin membrane, 80 nm thick, 5*5 mm^2, coated on both faces by 4,5 Mo:Si bilayers. These beamsplitters having a low internal stress, their flatness is deteriorated on the edges leading to the observed fringe deformation.
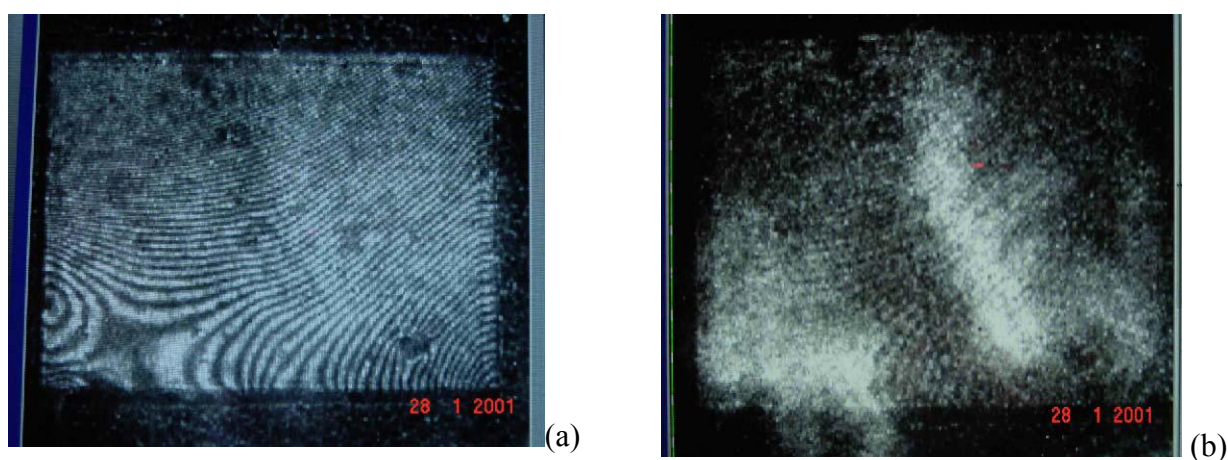

(a)   (b)

Figure 2 : Interferograms achieved with the Ni-like Ag x-ray laser. On the left image the interferometer arms were equilibrated while on the right one there was a path length difference of 200 µm.

By comparing the two interferograms we may observe a strong loss of contrast by increasing the path length difference. The left image having a contrast around 90% while it drops down to about 20% on the right image. It was quite surprising to observe that the loss of contrast was not constant through the x-ray laser beam cross-section. We then measured the contrast for different path lengths on the beam edges, where the fringes nearly disappeared on fig. 2b, and at the center. Figure 3 a and b display the fringe visibility curves and their Fourier-Transform curves, respectively. These last curves are the x-ray laser line-shapes (plain lines). The gaussian-like line-shape corresponds to the beam edges while at the beam center the line-shape looks like a Lorentzian. Following the experimental works, we have performed several numerical modellings. Intrinsic line profile of the Ag XRL is calculated in the framework of the frequency-fluctuation model [8] which takes into account the dominant broadening mechanisms : Doppler, natural and collisions as well as gain-narrowing. The first analysis seems to show that the whole beam was not emitted in the same region. Indeed, the estimated electron density was in the range of 10^{20} cm^{-3} for the Lorentzian-like line-shape and around 10^{21} cm^{-3} for the gaussian-like. Further investigations are required for explaining this result.

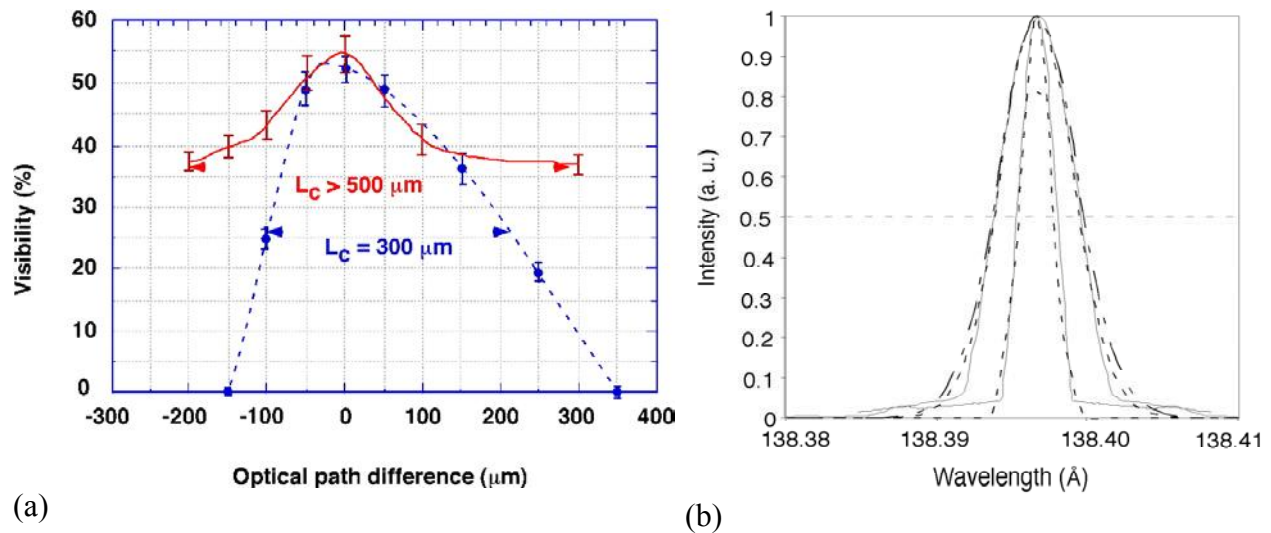<p align="center">(a)   (b)</p>

Figure 3 : On the left, visibility curves are measured at the beam center (plain line) and the beam edge (dashed). On the right, the line-shapes are displayed. Plain lines are experimental curves while dotted ones are coming from the modelling. Again the gaussian-like line is coming from the XRL beam edge.

The second run of experiments has been performed in collaboration with the J. Dunn's group from LLNL. The main results being published in that proceeding (Dunn et al), we will only show the measured XRL line-shape. The Ni-like Pd 14.68 nm x-ray laser beam was generated using two laser beams at 1054 nm wavelength from the Compact Multipulse Terawatt (COMET) laser facility at LLNL [3]. Saturated x-ray laser was achieved with a combination of a 600 ps long pulse (2 J, 2×10^{11} W cm^{-2}) and a 13 ps (5 J, 3×10^{13} W cm^{-2}) main heating pulse. The short pulse arrived 700 ps peak-to-peak after the long pulse. For some shots the duration of the picosecond pulse was shortened to 6ps (5 J, 6×10^{13} Wcm^{-2}). The whole experimental setup including the Michelson interferometer was slightly different from the LULI experiment, particularly because a spherical mirror was used for magnifying the XRL beam by a factor of 7. So, comparison between LULI and COMET interferograms can not be done straightforward. On figure 4, it is displayed the measured fringe visibility curves for x-ray lasers pumped by a 6 or a 13 ps driving laser. It is interesting to note that the curve width is somehow larger for the longest driving pulse, leading to a smaller line-width, as coming from different plasma conditions during XRL emission and amplification.
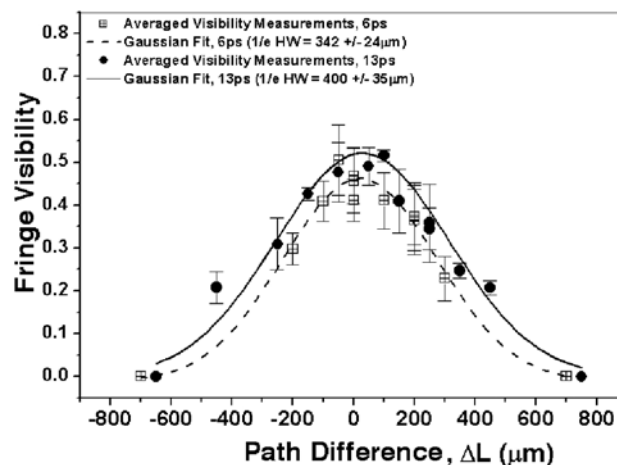

Figure 4: Variation of fringe visibility with path difference between two arms of the interferometer for 6 ps (open symbols) and 13 ps (closed symbols) heating pulse. Each data point is average visibility for a given shot taken from nine separate measurements across the interferogram. Error bars represent one standard deviation. The data points are fit by a Gaussian curve with a 1/e half width (HW) of 400 μm ± 35 μm (solid line, 13 ps) and 342 μm ± 24 μm (dashed line, 6 ps).

Our most recent work has been to improve the beamsplitter flatness by changing the coating process. Although fringe deformation is not deleterious for contrast measurement it might be problematic for applications requiring a large field of view, like some plasma probing experiments or optic metrology. Thanks to the use of a new magnetron sputtering machine (instead of the older ions sputtering) we were able to easily change the coating parameters and then improve the flatness. Layer thickness, ratio between Mo and Si thickness, coating speed are some of the tested parameters. Since the flatness of a thin membrane is ensure by the tensile stress, we tried to keep the initial one at the highest value. Si_3N_4 membrane has a stress around 1 GPa which dropped to 100 MPa after coating the oldest beamsplitters. With the recent coating, the stress was kept to about 700 MPa. The beamsplitters flatness was measured by means of a commercial wavefront sensor (Shack-Hartmann). The oldest beamsplitters have a deformation of about 180 nm root-mean-square (rms), leading to about 15 residual fringes. Now over a 3*3 mm^2 surface, the beamsplitter is flatter than 4 nm, leading to a deformation of about a quarter of fringe.

3. XUV WAVEFRONT MEASUREMENTS

During this last years, wavefront measurement has been one of the major fields of research for visible lasers. Indeed, in the race of achieving higher and higher intensity, no one may accept a focal spot having most of the energy spread out. The loss of intensity from a focal spot achieved with uncorrected beam from a diffraction-limited one may easily reaches several orders of magnitude. For visible wavelength range, most of the recent development in improving the wavefront of focused beam have been concentrated on the laser itself because it is quite easy to buy a diffraction-limited optic. We would like to remind that according to Marechal criterion, a diffraction-limited beam should have a wavefront error lower than $\lambda/14$ rms, λ being the laser wavelength. However, due to the strong wavelength shortening it is quite difficult to make a diffraction-limited XUV optic. Researches on EUV lithography [9] has boasted the development of high quality optics but they are still very expensive and long to make. Consequently, regarding x-ray laser applications we have to take care at both the optics and the XRL wavefronts.

Many kind of wavefront sensors have been developed so far in the visible range, some being easy to transfer to the XUV wavelength range. Interferometers intrinsically measure a wavefront. However, most of them are recombining the beam onto itself making difficult the achievement of an absolute phase map. Also, fringe spacing is generally linked to the wavelength imposing to realign the interferometer after any wavelength change. This make interferometers poorly versatile. Another kind of wavefront sensors is based on ray propagation. The principle displayed on figure 5 is simple. The beam is sampled by splitting it into many beamlets (by using a hole or lens array). All the beamlets are considered to have a flat but tilted wavefront. The position of each beamlet spot onto the detector gives directly the angle of the wavefront tilt at the position of the hole or lens array. Then, if the beam is coherent, we may integrate all the wave vectors and reconstruct the wavefront. If the beam is partially coherent this last step has no physical meaning and then we just achieve a map of the wave-vectors. This kind of wavefront sensors, called Hartmann for the hole array and Shack-Hartmann for the lens array, are very simple and robust. There is no chromatic effect which make them very versatile.

Some years ago we have developed the first XUV wavefront sensor based on the Shack-Hartmann technique [10] The lenses were replaced by Fresnel lenses (also called zone plates) which are diffractive, focusing optics. Normally, they are composed of concentric ellipsoids, some blocking the light some being transparent. Due to the high absorption of most materials in the wavelength range of interest we use reflective Fresnel lenses. These lenses are made by etching a photo-resist coated onto a silicate substrate, the ellipsoids being written by a electron beam. After the etching phase, the whole substrate is coated with a reflective interferential multilayer (Mo:Si). Then all the ellipsoids are reflecting the incoming beam. By adjusting the depth of two consecutive ellipses, the wave phase is perturbed such as making a convergent beam and then a focal spot. The detector was a back-illuminated thinned CCD sensitive to XUV light. The most critical part of the Hartmann or Shack-Hartmann techniques is the focal spot position retrieval. We have developed a software able to find the spot position with an accuracy of about 1/100 of pixel. Then as coming from the distance from the lens array to the detector, we estimated the wavefront accuracy at about $\lambda/100$ at 13 nm.
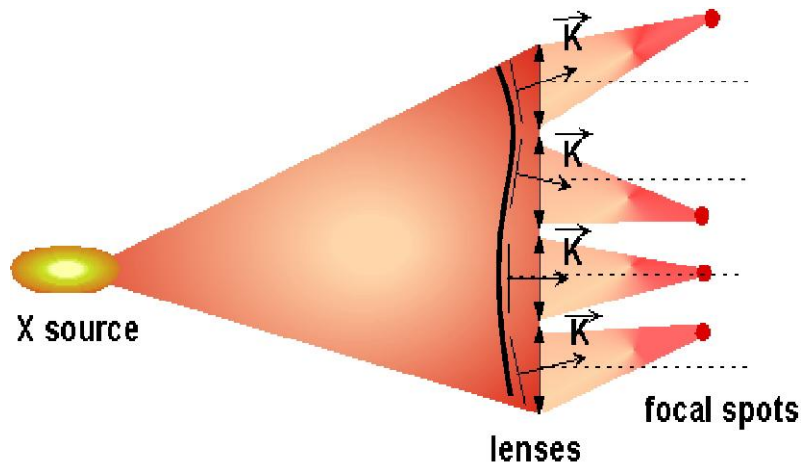
Figure 5 : Schematic diagram of a Shack-Hartmann wavefront sensor. The local wave-fronts as well as the local wave-vectors are displayed.

Our first study has been to measure the wavefront of several collisional x-ray lasers. We have worked with both laser-pumped and capillary discharge XRLs. For laser-pumped we measure the beam quality of XRLs pumped by 600ps, 130 ps and 20 fs infrared lasers. The last XRL is generated by OFI. For the longest driving laser case, we also study the effect of using a half-cavity for re-injecting the beam into the plasma. We will only summarize the experimental results.

To our knowledge, laser-pumped XRL are not or poorly coherent (spatial coherence) meaning that wavefront has no meaning. Then we perform maps of the wave-vectors for all the cases. For XRLs generated from a solid target the beam quality is quite poor (equivalent to about 10λ rms for a wavefront deformation) as given by the wide dispersion of the wave-vector angles. The reason is probably coming from the large electron density gradients experienced by the XRL while propagating along the plasma. However, these gradients which are known to be responsible from beam deflection may deteriorate the beam quality only if the electron density changes over small scales. We did not perform enough study to ensure the origin of these small-scale variations but we may point out some possibilities. Laser-generated plasmas are known to be the place of many instabilities (parametric and hydrodynamic). Hydrodynamic instabilities may start from the target roughness, for example. Filamentation is a parametric instability, coupling between plasma waves and the driving laser, which generates dips in the plasma. Filamentation threshold is in the range of 10^{12} Wcm^{-2} which is about one order of magnitude lower than the mean pumping intensity. The hypothesis that the XRL beam is degraded by the plasma density variations is reinforced by the measurement of a very good beam quality for OFI laser which is emitted in a low density and consequently weakly refractive plasma.

Capillary discharge, 46.9 nm XRL (Ne-like Ar) has been studied for different conditions of production. We first study the influence of the plasma length onto the wavefront quality. Previous measurements have shown a dramatic improvement of the beam coherence by increasing the plasma length [11]. However, we would like to remind that there is no intrinsic correlation between wavefront and coherence preventing for using the coherence measurements for any estimation of the wavefront quality. On figure 6 it is displayed the wavefront (a) and intensity map (b) as measured by the wavefront sensor for a 18 cm long plasma. For this length the XRL just reach the saturation regime. We observe a smooth but strongly distorted phase. The intensity is annular.
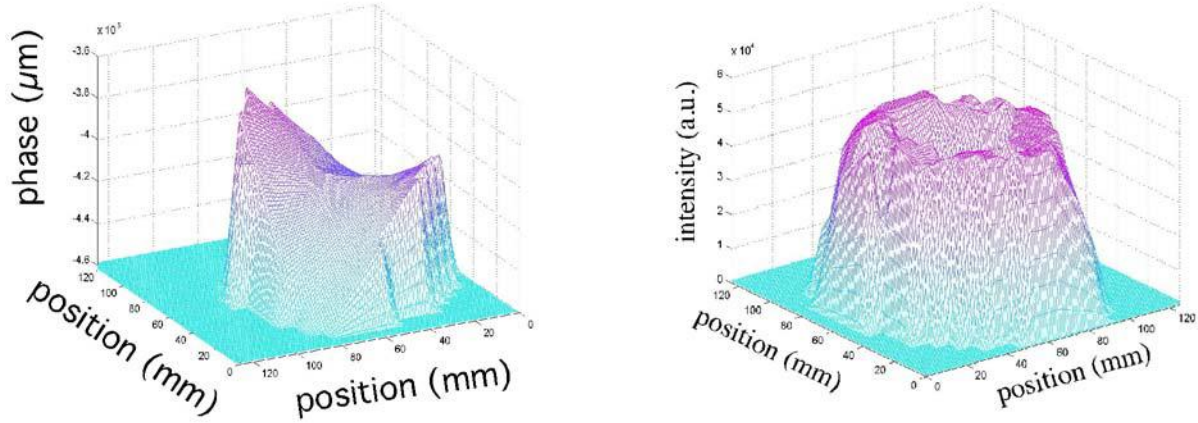
(a)   (b)

Figure 6 : XRL wavefront (a) and intensity (b) maps as measured at 2.5 m from the end of a 18 cm capillary.

From these two data we may fully reconstruct the XRL electric field and then by Fourier-transform estimate the intensity distribution at a theoretical focal plane. We consider here a 5 cm focal length. The focal plane intensity map is displayed on Figure 7. We may observe a central peak surrounded by several smaller peaks and also light spread far away. We then estimated that about 5% of the incident energy was in the central peak of 3 μm in diameter which corresponds quite well to the measurement achieved by B. R. Benware et al in the same conditions [12].
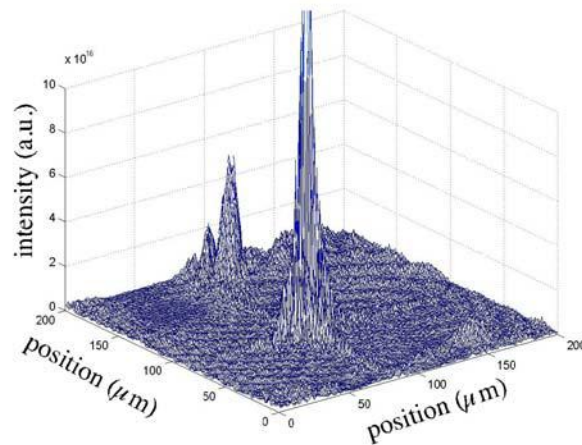

Figure 7 : Theoretical intensity distribution at the focal plane of a perfect focusing optic with f = 5 cm and considering the beam parameters displayed on fig. 6

While elongating the plasma up to 36 cm, the beam improvement might be observed on the map displayed below (fig. 8 a), showing a smooth wavefront. It is interesting to note that the wavefront is roughly spherical and divergent. The electron density being higher at the capillary center than on the edges, the plasma behaves like a divergent lens, generating a divergent wavefront. Since most of the x-ray laser rays are pushed out of the central gain region of the plasma while propagating, the beam is more and more filtered with increasing the plasma length. This explains the good quality of the wavefront that is better than 1.5λ rms. The Fourier-transform of the associated electric field shows a clean focal spot, 0.5 μm FWHM (fig. 8 c). The intensity is then estimated to be around 5×10^{13} Wcm^{-2}.
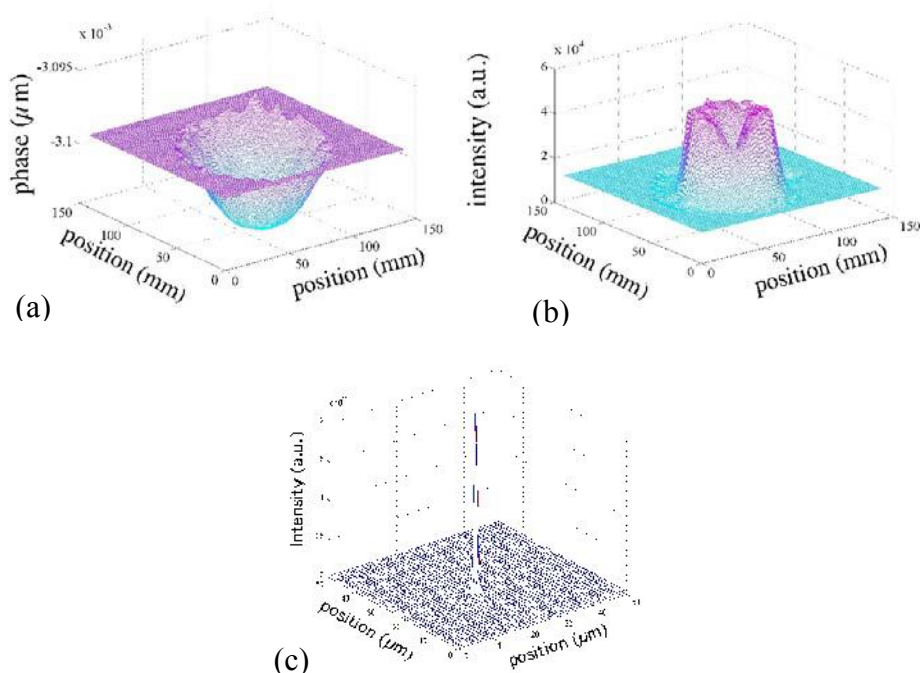
Figure 8 : Wavefront (a) and intensity (b) maps of a 36 cm long capillary x-ray laser. Fig. 8c shows the theoretical focal spot as calculated with these experimental data and considering a f = 5 cm focusing mirror.

One of the main difficulty while using a Hartmann or Shack-Hartmann wavefront sensor is the need of pre-calibrating it. Indeed as explained previously, the focal spot barycenter is retrieved with an accuracy of 1/100 of pixel i.e. 0.2 μm. Considering that for wavefront reconstruction, the relative position between all the spots is important and with a number of spot ranging from 20*20 up to 60*60 typically, one may understand that is impossible to mechanically ensure the absolute position of each spots. Commonly to calibrate the sensor one use a well-known wave, for example generated by the diffraction of a pinhole. The typical size of the pinhole is around 1 μm depending of the diffracted beam optical aperture needed. Previous work has shown that the wavefront is better than λ/100 over a disk half the diameter of the Airy ring [4], centered on it. Attention has to be paid to that phase since the accuracy of the wavefront sensor will be obviously limited by the quality of the calibration wave. It is better to calibrate the sensor on a short exposure time (1 s or shorter) meaning that the diffracted wave has to be of high average power. Due to the use of a tiny pinhole, it is preferable to focus the incoming light onto the pinhole to increase the transmitted power. Consequently, a high power XUV source is required for calibrating a wavefront sensor. For this task, under a collaboration between Imagine Optic firm, Center for X-ray Optics and LIXAM, we used the beamline 12.0 of the 3rd generation synchrotron ALS. This beamline is based on an undulator ensuring a high power. Beamline 12.0 being commonly used for interferometric measurement with a point-source interferometer, most of the set-up was already existing (pre-focusing, pinhole…). The diagram displayed on fig. 9 shows the beamline geometry as well as the implementation of the wavefront sensor. The beam is first monochromatized and then focused onto the pinhole by a Kirkpatrick-Baez optic. For this work, we used a hole array to sample the beam. Indeed a hole array is more simple to manufacture than diffractive lenses. Also the use of a hole array makes the sensor completely achromatic. Diffractive lenses present the strong disavandtage that their focal lengths depend on the incoming beam wavelength, making the sensor poorly versatile. The undulator was mainly run at 13 nm but we also test our wavefront sensor from 6 to 25 nm.
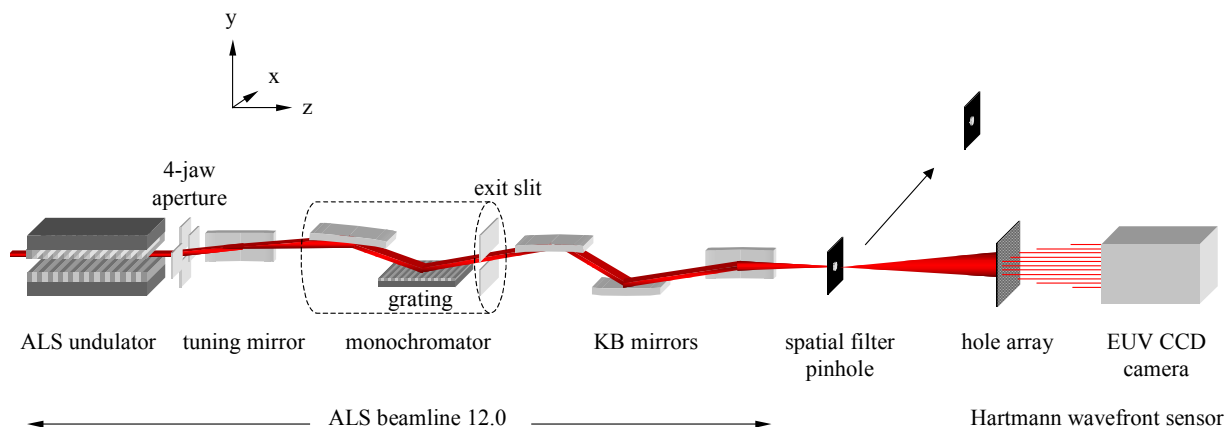
Figure 9 : Diagram of the beamline 12.0 at the ALS synchrotron facility as it was used for Hartmann sensor calibration. The pinhole was inserted for calibration and was removed for measurement of the beamline wavefront.

Estimation of the sensor accuracy has been made by comparing the wavefronts generated by the diffraction of the pinhole on two independent measurements. The accuracy is around $\lambda/120$ rms at 13 nm with a sensitivity exceeding $\lambda/1500$ rms. Note that the best interferometers demonstrated an accuracy around $\lambda/300$ but with a more sophisticated set-up. We measured the accuracy over the 6-25 nm wavelength range and observed no noticeable loss of accuracy.
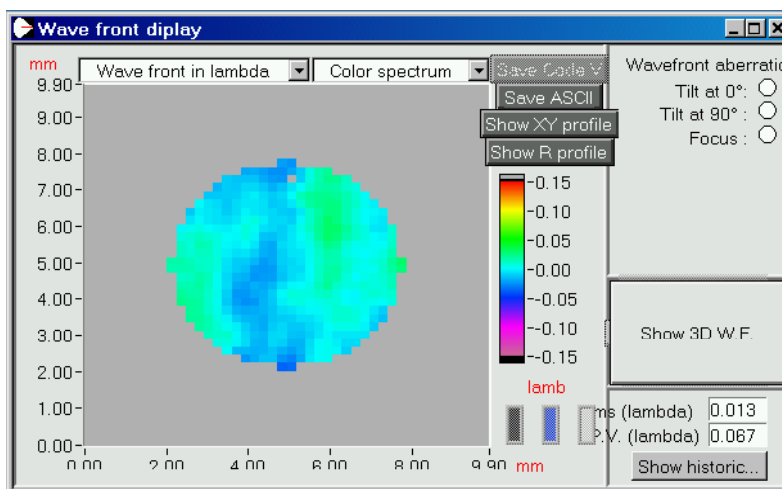

Figure 10 : Pinhole diffracted wavefront, measured after calibration of the sensor. The tilt and defocus terms were removed.

After the calibration phase, the pinhole was removed enabling us to measure the wavefront of the unfiltered beamline. The result is displayed on fig. 11 a. We observed that the main aberration is the astigmatism probably coming from a slight misalignment of one or two mirrors of the Kirpatrick-Baez. From the wavefront measurement, the Imagine Optic software calculates the focal spot (fig.11 b) which is quite close to what we measured directly. The spot is elliptic ($10{\times}20~\mu m^2$) as coming from the astigmatism. Since the software displayed the value of each Zernike polynomials, it is quite easy to use the wavefront sensor for precisely aligning an XUV optic. Unfortunately, in that case we were not able to access to the alignment stages.
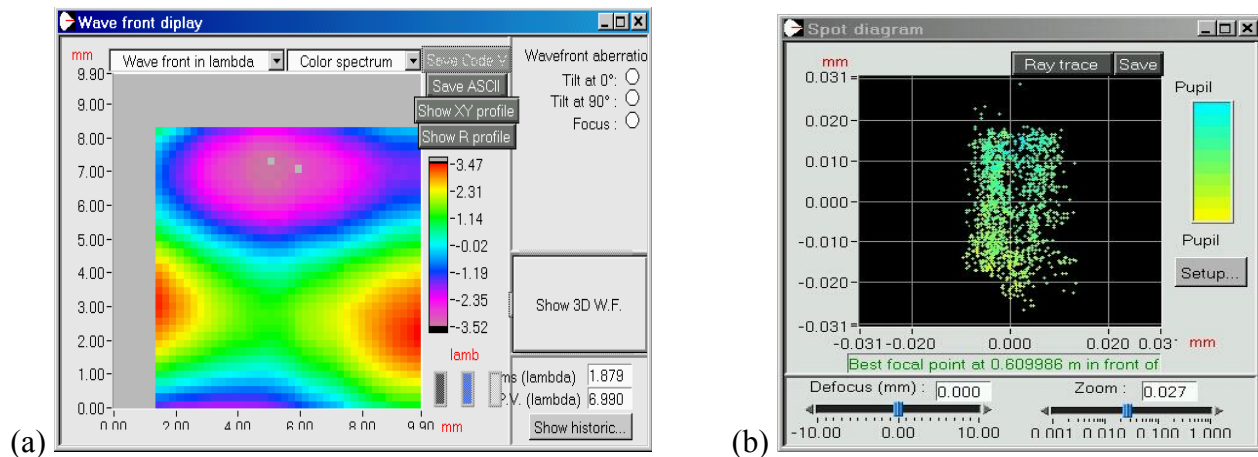
Figure 11 : Image of the experimental Beamline 12.0 wave front (a) showing the astigmatism, and the focal spot (b) as calculated from the experimental data.

Further development of XUV wavefront sensors specially their commercialization will require to easily access to a source like the beamline 12.0 having a "perfect" wavefront for calibration. Beamline 12.0 being heavily used for lithography projects, the access time will be low. That is why, we are planning to set-up a coherent XUV beamline at the Laboratoire d'Optique Appliquée-France. As pointed out the main parameters are the wavefront quality, the average power and the possibility to tune the wavelength, typically from 10 to 60 nm. Obviously considering an industrial use of the future beamline, the beam stability and the easiness to run will be two key parameters. At the moment x-ray lasers do not response to our needs (low rep-rate, low average power, no tunabillity). High harmonic generation (HHG) corresponds quite well to all our requirements. The driving laser, Ti:Sapphire, is running at 1 kHz and might be up-graded to several kHz. HHG are known to be fully tunable and the average power is not too low. Typically on beamline 12.0 the power is around 10 µW at 13 nm after the spatial filter and from previous LOA works [13], it is estimated at 6 µW with the HHG at 30 nm. The power drops at 6 nW around 13 nm but we never optimized the HHG flux in this wavelength range. We may expect to increase this value by more than one order of magnitude after optimization and by increasing the laser rep-rate. Also, reminding the ALS experiment, one can understand that average power might be easily enhanced by tightly focusing the beam onto the pinhole used for spatial filtering. At ALS the transmission is as low as 1/100 because the focal spot is large. Thanks to good quality of the HHG wave front, we may expect to generate focal spot as small as 1 µm in diameter, leading to weak losses.

Tight focusing of the HHG requires to use a good quality optic for keeping the wavefront as good as possible. For generating a focal spot with diameter around 1 µm, the focal length has to be short (5-10 cm). Also due to the need of placing a pinhole at the focal spot, the beam can not go downstream like when a spherical mirror is used in normal incidence. Short focal, grazing incidence mirrors are generally not so good leading to distorted focal spot [14]. Sophisticated grazing incidence focusing optics correcting the aberrations are feasible but are quite expensive. One of them will be set-up for the future LOA/LIXAM beamline. However, for the first work we decided to use an off-axis parabola enabling to shift, without distortion, the focal spot out from the incoming beam path. In sake of alignment easiness the full parabola was polished while just a small part (off-axis) has been polished to the required quality (λ/30 rms, λ = 632.8 nm). By placing a luminescent crystal (YAG:Ce) in place of the focal spot we measured the intensity repartition at the focal plane. The parabola was coated with a 1000 Å Cr layer in order to keep the focused intensity at a low level, preventing for damaging the crystal. The YAG green emission was magnified by a lens doublet (*30) and recorded onto a CCD. Due to the YAG non-linearity response versus HHG intensity the raw image has been corrected. Figure 12 shows the final image of the achieved focal spot. The spot is nicely circular showing that aberrations have been kept at a negligible level. The spot diameter is around 2.5 µm.
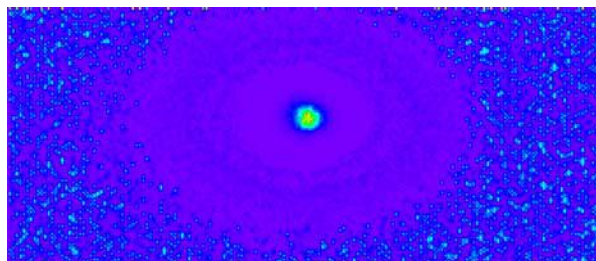
Figure 12 : Corrected image of the focal spot obtained by focusing the HHG with an off-axis parabola (f = 7 cm) onto a luminescent crystal. The focal spot diameter is around 2.5 µm.

4. CONCLUSION

In the aim of developing X-ray laser facilities dedicated to applications, achievement of high quality XUV optics or optical systems is necessary. We have developed XUV beamsplitters through the realization of a Michelson interferometer. At the moment the beamsplitter flatness is better than 4 nm over a 3*3 mm^2 surface. Michelson has been used to conduct a large study on x-ray laser line shape considering several conditions of pumping (long pulse and transient). Fourier-Transform spectroscopy (with the Michelson) is a very sensitive tool for studying the x-ray laser generation and amplification processes in plasmas.

We also developed the first XUV wavefront sensor enabling us to study the beam quality of many x-ray lasers. X-ray laser generated by a solid target do not exhibit a good wavefront as probably coming from plasma instabilities. Capillary discharge XRL have a very good wavefront ensuring that tight focusing is possible. Most recent developments of XUV wavefront sensors have consisted in measuring their absolute accuracy (λ/120 at 13 nm). The first step for setting up a coherent XUV optic beamline has been to demonstrate that micrometer focusing is possible with HHG.

REFERENCES

1.   L.B. Da Silva et al, Phys. Rev. Lett., **74**, 3991 (1995)
2.   D. Joyeux, F. Polack, D. Phalippou, Rev. of Sci. Inst., **70**, 7, 2921 (1999)
3.   B. Rus et al, Proc. of the 8th Int. Conf. On X-ray Lasers, Aspen, 2002, ed. J.J. Rocca, J. Dunn, S. Suckewer, AIP, **641**, p522
4.   H. Medecki et al, Opt. Lett., **21**, 1526 (1996)
5.   A. A. Michelson, *Phil. Mag.* **34**, 280 (1892)
6.   J. W. Goodman, *Statistical Optics* , Wiley, New York, 1985, 74
7.   S. Sebban et al, Phys. Rev. A, **61** (2000)
8.   B. Talin et al, Phys. Rev. A, **51**, 3 (1995)
9.   D. Attwood, *Soft X-rays and Extreme Ultraviolet radiation, principles and Applications*, Cmabridge University Press, 1999
10. S. Le Pape et al, Phys. Rev. Lett., **88**, 18 (2002)
11. Y. Liu et al, Phys. Rev. A. **63**, 033802-1, (2001)
12. B. R. Benware et al, Opt. Lett. **24**, 23, 1714 (1999)
13. S. Kazamias et al, Eur. Phys. J. D, Avril 2003
14. C. Valentin et al, Opt. Lett, **28**, 12, Juin 2003.